Computational modeling of solid tumor growth: the avascular stage

Didier Bresch, Thierry Colin, Emmanuel Grenier, Benjamin Ribba, Olivier Saut

COMPUTATIONAL MODELING OF SOLID TUMOR GROWTH: THE AVASCULAR STAGE

DIDIER BRESCH *, THIERRY COLIN †, EMMANUEL GRENIER ‡, BENJAMIN RIBBA §, AND OLIVIER SAUT ¶

Abstract. In this paper, we present a mathematical model for avascular tumor growth and its numerical study in two and three dimensions. For this purpose, we use a multiscale model using PDEs to describe the evolution of the tumor cell densities. In our model, cell cycle regulation depends mainly on micro-environment. The cancer growth of volume induces cells motion and tumor expansion. According to biology, cells grow against a basal membrane which interacts mechanically with the tumor. We use a level set method to describe this membrane and we compute its influence on cell movement thanks to a Stokes equation. The evolution of oxygen, diffusing from blood vessel to cancer cells and used to estimate hypoxia, is given by a stationary diffusion equation solved with a penalty method. The model has been applied to investigate the therapeutic benefit of anti-invasive agents and constitutes now the basis of a numerical platform for tumor growth simulations.

Key words. Avascular tumor growth. Multiscale models. Cell cycle modeling. Fluid dynamics. Level-set methods.

AMS subject classifications. 65M06 ; 76Z99 ; 92B99.

1. Introduction.

Small tumors appear when cells lack of growth control. Uncontrolled proliferation can be the result of different alterations of normal cells properties (see [31] for a review). In particular, disruption of cell cycle can lead cells to proliferate without limitation leading to the formation of an initial tumor nodule.

To proliferate, cells need nutrients and oxygen coming from existing vascular vessels surrounding the tissue where the tumor grows. It is well known that the process of cancer growth can be divided into two stages [8]. The first stage is the avascular stage where the cells receive nutrient and oxygen from existing blood vasculature. Avascular tumors can grow until the lack of nutrient and oxygen limits the extension of the initial nodule. An avascular tumor can not grow over 10^6 cells. Starving cells have the ability to secrete vessel chemoattractants in order to induce the formation of new blood vessels towards the tumor. This is called the process of angiogenesis [8]. When a tumor is able to induce angiogenesis, it can become vascularized. Vascular tumors are much less limited in terms of nutrient and oxygen and can metastasize to distant organs through cells penetration into the newly formed blood vessels. One can found many mathematical models describing vascular growth of tumors [4, 36, 38, 42].

In this paper, we will focus on the avascular stage where the regulation of the cell cycle is among the most important factors. It is known that the progression in the cell cycle is conditioned by the tumor microenvironment. If the environment

*Lama, Université de Savoie, CNRS UMR 5127, Campus scientifique, 73376 Le Bourget du lac cedex, France, (Didier.Bresch@univ-savoie.fr)

†Université Bordeaux 1, Institut de Mathématiques, INRIA Bordeaux-Sud Ouest MC2, 351 cours de la libération, 33405 Talence Cedex, France, (Thierry.Colin@math.u-bordeaux1.fr)

‡Unité de Mathématiques Pures et Appliquées, CNRS UMR 5669, Ecole Normale Supérieure de Lyon, 69364 Lyon cedex 07, France, (Emmanuel.Grenier@umpa.ens-lyon.fr)

§Université de Lyon, Lyon, F-69003, France; Université Lyon 1, Ciblage Thérapeutique en Oncologie (EA3738), Faculté de Médecine Lyon-Sud, Oullins, F-69921, France, (Benjamin.Ribba@recherche.univ-lyon1.fr)

¶Université Bordeaux 1, Institut de Mathématiques, CNRS UMR 5254 and INRIA Bordeaux Sud-Ouest MC2, 351 cours de la libération, 33405 Talence Cedex, France, (Olivier.Saut@math.u-bordeaux1.fr)

conditions are not adequate (*e.g.* lack of nutrient) the progression is stopped and the division process ceases [8, 2]. Furthermore, it is quite clear that the macroscopic aspects including mechanical constrains and tissue deformation play a significant role in tumor growth and therefore, there should be complex interactions between the macroscopic level (tissue level) and the cell cycle regulation (cell level).

There is a significant number of mathematical models representing tumor growth through the regulation of cell cycle as well as the macroscopic and tissue level. However, these two factors are somehow separated. Indeed, macroscopic models of tumor growth integrating tissue mechanical constraints generally do not integrate precisely molecular or cellular events occurring during cell cycle regulation. For a complete description of mathematical describing avascular tumor growth, one can see [47].

The present highly integrated framework has been initiated in [45], where moreover, genetic level was taken into account. In [46], we showed the significant potential of this approach to investigate recent therapeutic developments.

We use a macroscopic model as cell-based models as [1, 37] are computationally expensive and have difficulties rendering mechanical effects. Yet, the cell-based models are adequate to describe the smaller scales and for instance to account for genetic regulation [5]. Macroscopic models describe the mean evolution of a large number of cells and are probably more adapted to describe large tumors.

A large number of macroscopic models are based on mass-balance equations written for each cellular density [14]. In these equations, one has to compute the cellular flux representing cell movement and cell birth/death as sources terms. In several models, the motion of cells is described using a nonlinear diffusion term [48]. These models are well adapted to describe some interplay between cells (such as contact inhibition) but can not really account for the influence of an elastic membrane. The models based on diffusion equations involve few parameters to determine and have been successfully used for evaluating the efficacy of therapy or resection in the case of brain tumors for instance [49] or the influence of acidity [28, 29] (let us note that adding acidity to our model is done in [13]). However, the expressions of the nonlinear diffusion coefficients (which describe the interaction between different cellular types) of these models can be difficult to justify. Furthermore some of these models do not consider the influence of nutrients or mechanical effects.

One can also describe the flux as an advection term [22] where the velocity of cells is computed assuming a potential flow [3]. The model presented in this paper belongs to the same class of models, the so-called "mechanical" models.

Finally, another approach can be used. The tumoral growth can also be obtained from the evolution of its boundary [35, 21]. Some of these models can be studied mathematically [27]. This approach is very efficient from a computational point of view. These models have been successfully coupled to models of neovascularization [21]. Yet, accounting for the mechanical effects and heterogeneity of the extracellular medium is more difficult than with models based on cellular densities. Furthermore, one has to define the tumor boundary which is not obvious in *in vivo* experiments. Recently a mixture model [20] was proposed to overcome many of these limitations.

Here, we describe with more details the mathematical and computational model which will constitute the basis for further therapeutic investigations through successive biological components integration.

The model is a multiscale model based on a set of PDEs to describe avascular growth. The tumor will be described by the densities of cells (or numbers of cell per volume unit) in the quiescent and proliferating phases evolving in time and age in

the cell cycle (the set of transformations a cell has to undergo in order to divide). Hence, these densities are governed by equations with an advection term in space (corresponding to the movement created by the cellular division) and an aging term as the cells progress in the cell cycle. The transition between phases and cellular division will be accounted for through the boundary conditions in these equations.

The transition between quiescent and proliferating phases is controlled by environmental regulation signals. Our model takes into account two signals influencing cancer growth. The first one, *overpopulation*, is activated when there is not enough free space for cells to proliferate. The second one, *hypoxia*, is due to the lack of oxygen. Both signals have been shown to play a significant role in tumor growth [8, 2].

In the model, tumor cells are surrounded by a basal membrane. This membrane may slow the cancer growth. To describe the mechanical force of the membrane on the tumor, we use the immersed interface boundary method [41], where the membrane is represented by a level set function [39]. From this level set function, we compute the elastic force adapting a method from Cottet and Maître [17]. This force appears as a source term in the Stokes equations that we use to compute the velocity and pressure. In the vicinity of the membrane, cancer cells release matrix metalloproteinases (MMP), which are enzymes able to degrade the components of the basal membrane [46].

This paper is organized as follows. In Section 1, we present our model. In Section 2, we present the numerical schemes used to discretize this model. Finally, in Section 3, we perform various numerical experimentations.

2. Description of the model. In the following, we are interested in the experimental setup described in Figure 2.1. We consider the case of a growing cluster of cancer cells in a square domain containing a source of oxygen and a basal membrane.

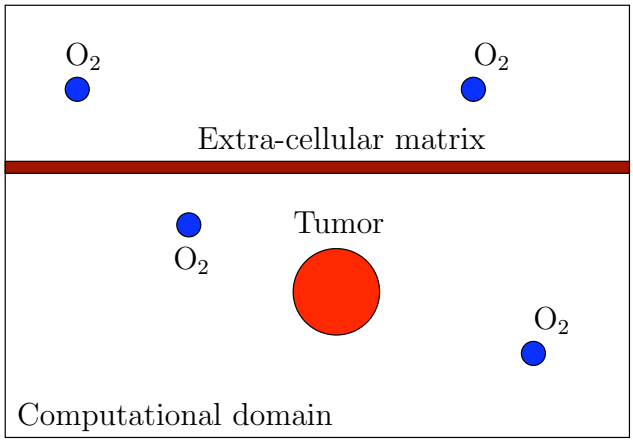

FIG. 2.1. *Experimental setup considered in this paper.*

2.1. Cellular description. Two different cell densities will be considered as tumor cells can be in two states. The proliferating one, where cells divide, leads to the tumor growth. And according to our hypothesis, if the environmental conditions are unfavorable, cells turn to a quiescent state, in which cellular division no longer occurs. We assumed that a cell can stay in a quiescent state forever. However, if

the environment changes to be favorable again, cells can return to the proliferating state. The environmental conditions are checked at one point in the cell cycle: the *restriction point* [12].

The mathematical description is achieved through an age-structured model of the cell cycle [24, 23]. Cells evolve with respect to time t and to age a. We use a simplified model with two proliferating phases (whose densities per unit volume are denoted by P_1 and P_2) and one quiescent phase (denoted by Q). Note that the variables P_1 and P_2 depend on time, space and age (t, x, y, z, a) while Q only depends on time and space (t, x, y, z) (since we assume that cells do not evolve in age in the quiescent phase). The cycle is summarized in Figure 2.2. The durations of the phases P_1 and P_2 are denoted by $a_{\max,P_1}$ and $a_{\max,P_2}$ respectively. They can be evaluated from the literature [43, 44].

FIG. 2.2. *Principle of the simplified cell cycle considered in this paper. The transition between phases P_1 and P_2 is controlled by the boolean function f at the restriction point.*

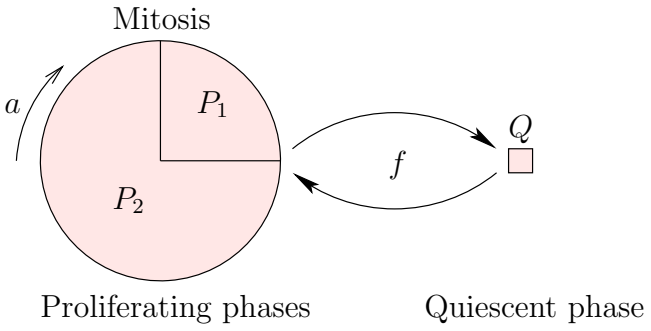

2.2. Environmental conditions. In the model, two factors regulate cell cycle transitions. The first one is related to the total cell density. If this density is above a particular threshold, we consider that proliferating cells become quiescent. The second one is the oxygen concentration. As before, if this concentration is below a particular threshold, we consider that proliferating cells become quiescent. Therefore, at each point of the computational domain, we compute the number of cells and the quantity of oxygen that is available.

In order to describe these tests quantitatively we introduce the following boolean function

$$f(t,x,y,z) = \begin{cases} 1 & \text{if } \int_0^{a_{\max,P_1}} P_1(t,x,y,z,a)da + 2\int_0^{a_{\max,P_2}} P_2(t,x,y,z,a)da \\ & \quad +Q(t,x,y,z) < \tau_o \text{ and } C(t,x,y,z) > \tau_h, \\ 0 & \text{otherwise,} \end{cases} \tag{2.1}$$

where τ_o is the cancer overpopulation threshold, τ_h the hypoxia threshold. Here $C(t, x, y, z)$ denotes the concentration of oxygen at point (x, y, z) (see the equation (2.7) below). The factor 2 before the population of phase P_2 comes from the fact that the cells present in the second part of the cycle will divide and therefore contribute to the increase of volume.

The evolution of the population of cells in the cycle is described by

$$\left\{\begin{array}{lllll} \partial_t P_1 & +\partial_a P_1 & +\nabla\cdot(\mathbf{v}_{P_1}\,P_1) & = & 0,\\ \partial_t P_2 & +\partial_a P_2 & +\nabla\cdot(\mathbf{v}_{P_2}\,P_2) & = & 0,\\ \partial_t Q & & +\nabla\cdot(\mathbf{v}_Q\,Q) & = & (1-f)P_1(a=a_{\max,P_1}) - \left[\frac{d}{dt}f\right]^+ Q(t^-), \end{array}\right. \tag{2.2}$$

where $\mathbf{v}_{P_1}$, $\mathbf{v}_{P_2}$, $\mathbf{v}_Q$ are the velocities of the three phases P_1, P_2 and Q respectively, which we shall determine later on. To describe the aging process, we have added a derivative on the age a as in [16]. We have denoted by $\left[\frac{d}{dt}f\right]^+$ the positive part of $\left[\frac{d}{dt}f\right]$. According to the third equation of (2.2), if the environment is not favorable, *i.e.* $f=0$, cells in the phase P_1 become quiescent and appear as a source term in the equation driving the evolution of the phase Q. If the environment is appropriate, *i.e.* $f=1$, these cells enter the phase P_2. If the environment has just turned to be favorable, the quiescent cells reenter a mitotic phase (P_2) and leave the quiescent phase. This transition is captured by the Dirac mass $\left[\frac{d}{dt}f\right]^+$.

To describe the transition between the cycle phases and the cell division, we write the following boundary conditions on the age a:

$$\left\{\begin{array}{l} P_1(a=0) = 2\,P_2(a=a_{\max,P_2}),\\ \\ P_2(a=0) = f\,P_1(a=a_{\max,P_1}) + \left[\frac{d}{dt}f\right]^+ Q(t^-). \end{array}\right. \tag{2.3}$$

The first equation of (2.3) corresponds to the cell division. The second one states that:

- If the environment is appropriate, the cells in the first age of the P_2 phase are cells previously in the last age of P_1.
- If the conditions change to be favorable, cells in the quiescent phase Q are added to the phase P_2 through the term $\left[\frac{d}{dt}f\right]^+ Q$.

As the cells do not evolve in age in the quiescent phases, the boundary conditions on Q appear as a source term in Eq. (2.2).

We also denote by M the density of normal cells or healthy tissue. This density evolves through an advection equation

$$\partial_t M + \nabla\cdot(\mathbf{v}_M \nabla M) = 0, \tag{2.4}$$

where we consider that healthy cells are not dividing relatively to the proliferative cells and that they do not die from environmental conditions (*e.g.* there is no apoptosis).

We will also assume that the total number of cells per unit volume is constant. This means that we consider cells as incompressible (which is certainly not always the case from the biological point of view, but we make this simplification here since for the time being it is out of reach to take into account the compressibility of the cells). Hence the following saturation assumption holds

$$M + Q + \int_0^{a_{\max,P_1}} P_1(a)da + \int_0^{a_{\max,P_2}} P_2(a)da = N_0, \tag{2.5}$$

meaning that the space is occupied by tumor cells or non-cancerous tissue where N_0 denotes the (constant) total number of cell per unit volume. Due to this condition, the density M can be directly obtained from the tumoral density and thus Eq. (2.4) will not be explicitly solved.

Since the system is mainly driven by the birth of new cells in the domain, we assume that the cells undergo a passive transport (and we neglect other possible types of cellular movement such as the diffusion of cells) and move at the velocity of a "surrounding" fluid $\mathbf{v}$. We therefore take $\mathbf{v}_{P_1} = \mathbf{v}_{P_2} = \mathbf{v}_Q = \mathbf{v}_M$ in (2.2) and (2.4). In [13], haptotaxy was added to this model.

Let us now differentiate Eq. (2.5) w.r.t. time and use equations (2.2), (2.4) and the boundary conditions (2.3). It is straightforward to see that it leads to a condition on the velocity $\mathbf{v}$ namely

$$\nabla \cdot \mathbf{v} = \frac{1}{N_0} P_2(a_{\max,P_2}). \tag{2.6}$$

The divergence of the velocity field is non negative. This corresponds to an increase of the volume of the tissue and will create a movement of the cells from the center of the domain to the boundary. The healthy cells are therefore "pushed out" through the boundary.

To determine the velocity $\mathbf{v}$, we need an additional equation on $\mathbf{v}$ to close the system (see section 2.4).

2.3. Distribution of oxygen. According to our model hypothesis, oxygen is essential to the division of cells. We shall describe its distribution at the point (x, y, z) and time t by its concentration $C(t, x, y, z)$. The oxygen undergoes a diffusion process and is consumed by tumors cells in proliferating phases, *i.e.* we neglect consumption in the quiescent state. As oxygen molecules are much smaller than cells, they are not affected by the motion created by the mitosis.

We assume that in a part O of the computational domain Ω, this concentration is fixed. One can imagine O being a network of blood vessel for instance. As an example, one can consider Fig. 2.1, Ω being the whole computational domain and O the sources of oxygen in blue.

We also make the adiabatic approximation : the diffusion process occurs on much smaller time scales that the cellular division. Therefore we suppose that the equilibrium is reached instantaneously. Collecting these assumptions yields the following elliptic equation on C

$$\begin{cases} -\nabla \cdot (K \nabla C) = -\alpha \left(\sum_{i=1,2} \int_0^{a_{\max,P_i}} P_i(a) da \right) C, \text{ on } \Omega \setminus \mathrm{O} \\ C = C_0 \text{ on } \partial\Omega, \\ C = C_{\max} \text{ on } \mathrm{O}, \end{cases} \tag{2.7}$$

where α is the rate of consumption by the proliferating cells and K is the coefficient of diffusion. We assumed this function K to be dependent on cells distributions and basal membrane. This function is fully described in the appendix A. Note that $C_{\max}$ is the concentration of oxygen in the blood, while C_0 is some reference value needed for the computation on the external boundary of the computational domain.

For the sake of simplicity, we have considered that quiescent and healthy cells do not uptake nutrient (their consumption is smaller than the one of proliferative cells). However, if necessary it could easily be added in Eq. (2.7).

2.4. Computation of the velocity. To determine the dynamics of the motion of the tumor, we have to compute the hydrodynamic variables namely the velocity $\mathbf{v}$ and the pressure P. Classically, they are obtained through a Darcy's law [46, 3]

which describes porous media flows which may approximate tumor growth. (In 2D, Darcy's law can even be derived from the 3D Navier-Stokes equations for a shallow flow between two plates [9] in the Hele-Shaw limit. In 3D, this is no longer the case and Darcy's law can not be derived from the Stokes equations.) For a complete comparison of Stokes and Darcy models, one can see [34]. Contrary to the Darcy model, the Stokes model includes viscous stress. In this paper we chose to use the Stokes system to describe the hydrodynamical variables:

$$-\nabla \cdot (\nu D(\mathbf{v})) + \nabla \left(P + \frac{2}{d} \nu \mathrm{tr}(D(\mathbf{v})) \right) = \mathbf{F}, \tag{2.8}$$

where $D(v)_{ij} = (\partial_j v_i + \partial_i v_j)$ is the deformation rate tensor, ν the viscosity (which will depend linearly on the tumor density in the sequel, see appendix A), $\mathbf{F}$ the force due to the membrane [41] and $d(= 2, 3)$ the dimension of space. This elastic force $\mathbf{F}$ is vanishing outside the membrane.

From (2.5), we know that the total number of cells is constant in the computational domain. As cells divide, they push their neighbors and other cells are leaving the domain at its boundaries. Hence, an adequate boundary condition has to be written for the velocity.

In particular, Eq. (2.6) leads to the compatibility condition

$$\int_{\partial\Omega} \mathbf{v} \cdot \mathbf{n} = \int_{\Omega} P_2(a_{\max}), \tag{2.9}$$

where $\mathbf{n}$ denotes the normal at the boundary of the domain Ω. Therefore Dirichlet-type boundary conditions can not be used. We overcome this difficulty as follows.

We decompose the velocity as $\mathbf{v} = \mathbf{w} - \nabla\psi$, where $\mathbf{w} \cdot \mathbf{n} = 0$ and $\psi = 0$ on $\partial\Omega$. We moreover impose $\nabla \cdot \mathbf{w} = 0$. Then the function ψ satisfies

$$\begin{cases} \Delta\psi = -P_2(a_{\max}), \\ \psi = 0 \text{ on } \partial\Omega. \end{cases} \tag{2.10}$$

On the boundaries of the domain, we have $\mathbf{v} \cdot \mathbf{n} = -\frac{\partial\psi}{\partial\mathbf{n}}$, which is known through Eq. (2.10). As for the tangential component of the velocity $\mathbf{v} \cdot \tau$, we choose to use a Neumann condition:

$$\partial_n (\mathbf{v} \cdot \tau) = 0 \text{ on } \partial\Omega. \tag{2.11}$$

2.5. Membrane. We wish to take into account the elastic force on the fluid that a membrane may produce. This force acts as a source term in the Stokes equations [17]. Note that the width of the membrane is neglected relatively to the tumor size.

2.5.1. Localization. Many methods are available for describing the motion of a membrane. Among these methods, we can cite: the Volume-of-Fluid methods, particles methods and level set methods. We choose to use a level set formulation [39] for its accuracy and because it is easy to implement.

The interface at time t, Γ_t is considered as the zero level set of a function denoted by $\phi(t)$ and moves with the velocity $\mathbf{v}$. More precisely,

$$\Gamma_t = \{\mathbf{x} \in \Omega,\, \phi(t, \mathbf{x}) = 0\}. \tag{2.12}$$

If the interface forms a closed curve, we assume that inside the interface, we have $\phi(t, .) > 0$ and $\phi(t, .) < 0$ outside.

The evolution of the level set function is given by the following equation

$$\partial_t \phi + \mathbf{v} \cdot \nabla \phi = 0, \tag{2.13}$$

where the initial datum is the signed distance to the interface (*i.e.* $\phi(0, \mathbf{x}) = d(\mathbf{x}, \Gamma_0)$) at the beginning of the simulation.

2.5.2. Degradation. The membrane is also degraded by the tumor cells. At time t, the degradation of a point (x, y, z) of the membrane will be described by the variable $\eta(t, \mathbf{x})$, whose values range from $-\infty$ to 1 according to the degradation ($\eta \leq 0$ meaning there is no longer a membrane at the point considered). While the degradation state η is only defined on Γ_t, we will extend it to the whole domain along the normals to Γ_t. Later on, we will show how to do it numerically.

The variable η evolves through

$$\begin{array}{l} \partial_t \eta + \mathbf{v} \cdot \nabla \eta = -\beta(\mathcal{M}), \\ \partial_t \mathcal{M} - \nabla \cdot (K_{\mathcal{M}} \nabla \mathcal{M}) = \alpha_{\mathcal{M}} \cdot \int_a (P_1 + P_2) - \alpha_{\mathcal{M}} \mathcal{M}, \end{array} \tag{2.14}$$

where the hyperbolic function β is described in the appendix A, $K_{\mathcal{M}}$ is a coefficient of diffusion and $\alpha_{\mathcal{M}}$ a production rate. Physically, the quantity $\mathcal{M}$ corresponds to the density of metalloproteinases enzymes produced by the tumor in the vicinity of the membrane. These enzymes attack the membrane and are also degraded by the organism at a rate denoted by $\alpha_{\mathcal{M}}$.

2.5.3. Elasticity. We shall now compute the elastic force from η and ϕ. We consider a two-dimensional membrane in a three-dimensional flow, we mainly follows the approach of [17]. The elastic energy of the membrane is given by

$$\mathcal{E}(t) = \int_{\Gamma_t} \eta^+(\sigma) E(\mathcal{T}(\sigma)) d\sigma,$$

where the elementary energy E is obtained from:

$$E'(\mathcal{T}) = T_0(\mathcal{T} - 1), \tag{2.15}$$

and $\mathcal{T}(\sigma)$ is the stretching factor of the surface at σ, see below equation (2.18) for the value. The elementary energy E is given by $E(\mathcal{T}) = \frac{T_0}{2}(\mathcal{T} - 1)^2$.

To obtain the elastic force $\mathbf{F}$, one uses the relation

$$\frac{d}{dt}\mathcal{E}(t) = -\int_{\Gamma_t} \mathbf{F} \cdot \mathbf{v}. \tag{2.16}$$

Given $\epsilon > 0$, let us define $\Delta_0 = \{\mathbf{x} \in \Omega : |\phi(0, \mathbf{x})| \leq \epsilon\}$ and $\Delta_t = \{\mathbf{x} \in \Omega : |\phi(t, \mathbf{x})| \leq \epsilon\}$. Denote by $\mathbf{X}(t, \xi_1, \xi_2, \xi_3)$ a parametrization of Δ_t such that $\mathbf{X}(0, \xi_1, \xi_2, 0) = \Gamma_0$, $|\partial_{\xi_i} \mathbf{X}(0, \xi)| = 1$, $i = 1, 2, 3$, $\partial_i \mathbf{X}(0, \xi) \cdot \partial_j \mathbf{X}(0, \xi) = 0$ if $i \neq j$ and

$$\partial_t \mathbf{X}(t, \xi) = \mathbf{v}(t, \mathbf{X}(t, \xi)). \tag{2.17}$$

For the sake of simplicity, we write $\mathbf{X}_{\xi_i}$ for $\partial_{\xi_i} \mathbf{X}$ from now on.

We have $\partial_t[\phi(t, \mathbf{X}(t, \xi))] = [\partial_t \phi](t, \mathbf{X}) + \nabla \phi(t, \mathbf{X}) \cdot \mathbf{v}(t, \mathbf{X}) = 0$ from Eq. (2.13) and (2.17). Hence $\phi(t, \mathbf{X}(t, \xi_1, \xi_2, 0)) = \phi(0, \mathbf{X}(0, \xi_1, \xi_2, 0)) = 0$. The surface Γ_t is therefore parametrized by $(\xi_1, \xi_2) \mapsto \mathbf{X}(t, \xi_1, \xi_2, 0)$.

The stretching of the membrane Γ_t at $\mathbf{X}(t,\xi)$ is given by

$$\mathcal{T}(\mathbf{X}) = |\mathbf{X}_{\xi_1} \times \mathbf{X}_{\xi_2}|. \tag{2.18}$$

In order to compute the elastic force on the tumor due to the membrane, this stretching has to be obtained from ϕ and η.

We define the jacobian J on Δ_t by

$$J(t,\xi_1,\xi_2,\xi_3) = \det(\mathbf{X}_{\xi_1}, \mathbf{X}_{\xi_2}, \mathbf{X}_{\xi_3}). \tag{2.19}$$

The jacobian evolves according to the equation

$$\partial_t J = (\nabla \cdot \mathbf{v}(t, \mathbf{X}(t,\xi)))\, J. \tag{2.20}$$

We will now prove that $|\mathbf{X}_{\xi_1} \times \mathbf{X}_{\xi_2}|(t,\xi) = J(t,\xi)|\nabla\phi|(t,\mathbf{X}(t,\xi))$. Indeed, we have

$$\partial_t(\mathbf{X}_{\xi_1} \times \mathbf{X}_{\xi_2}) = d(\mathbf{v}(t,\mathbf{X}(t,\xi)))\mathbf{X}_{\xi_1} \times \mathbf{X}_{\xi_2} + \mathbf{X}_{\xi_1} \times d(\mathbf{v})\mathbf{X}_{\xi_2}, \tag{2.21}$$

using equation (2.17). We have denoted the tensor $[\partial_j v_i]_{i,j}$ by $d(\mathbf{v})$.

The matrix $d(\mathbf{v})$ can be decomposed into $d(\mathbf{v}) = \frac{\operatorname{tr} d(\mathbf{v})}{3}\mathrm{Id} + S + A$, where S is symmetric with a vanishing trace and A is antisymetric (adapting the proof used in [17]). We also know that $\operatorname{tr} d(\mathbf{v}) = \nabla \cdot \mathbf{v}$. Eq. (2.21) yields:

$$\begin{aligned}\partial_t(\mathbf{X}_{\xi_1} \times \mathbf{X}_{\xi_2}) &= -S(\mathbf{X}_{\xi_1} \times \mathbf{X}_{\xi_2}) + A(\mathbf{X}_{\xi_1} \times \mathbf{X}_{\xi_2}) + \frac{2}{3}\operatorname{tr} d(\mathbf{v})\mathbf{X}_{\xi_1} \times \mathbf{X}_{\xi_2} \\ &= -[d(\mathbf{v})]^t(\mathbf{X}_{\xi_1} \times \mathbf{X}_{\xi_2}) + \operatorname{tr} d(\mathbf{v})\mathbf{X}_{\xi_1} \times \mathbf{X}_{\xi_2}.\end{aligned}$$

With (2.13) and (2.20), we can also write:

$$\begin{aligned}\partial_t(J(t,\xi)\nabla\phi(t,\mathbf{X})) &= \partial_t J(t,\xi)\nabla\phi(t,\mathbf{X}) - J(t,\xi)[d(\mathbf{v})]^t\nabla\phi(t,\mathbf{X}) \\ &= (\nabla\cdot\mathbf{v})J(t,\xi)\nabla\phi(t,\mathbf{X}) - J(t,\xi)[d(\mathbf{v})]^t\nabla\phi(t,\mathbf{X}).\end{aligned}$$

Initialy, we have $\mathbf{X}_{\xi_1}(0,\xi_1,\xi_2,0) \times \mathbf{X}_{\xi_2}(0,\xi_1,\xi_2,0) = [J(0,\xi)\nabla\phi](\mathbf{X}(0,\xi_1,\xi_2,0))$ which completes the proof.

At this stage, our expression for the elastic energy is:

$$\mathcal{E}(t) = \int_{\Gamma_t} \eta^+(t,\mathbf{X}) E\left(J(t,\xi)|\nabla\phi(t,\mathbf{X})|\right) d\xi_1 d\xi_2. \tag{2.22}$$

Then, we perform the change of variables $\mathbf{x}(t) = \mathbf{X}(t,\xi_1,\xi_2,0)$ using the Lagrangian parametrization of the surface and the expression of $|X_{\xi_1} \times X_{\xi_2}|$. Let us denote by $\overline{J}(t,\mathbf{x})$ the function defined by $\overline{J}(t,\mathbf{X}(t,\xi_1,\xi_2,\xi_3)) = J(t,\xi)$. Note that $\overline{J}$ satisfies

$$\partial_t\overline{J} + \mathbf{v}\cdot\nabla\overline{J} = (\nabla\cdot\mathbf{v})\overline{J}. \tag{2.23}$$

The expression of the elastic energy in Eulerian variables is therefore:

$$\mathcal{E}(t) = \int_{\Gamma_t} \eta^+(t,\mathbf{x}) E\left(\overline{J}(t,\mathbf{x})|\nabla\phi(t,\mathbf{x})|\right) \frac{\overline{J}^{-1}(t,\mathbf{x})}{|\nabla\phi(t,\mathbf{x})|} d\mathbf{x}.$$

As in [17], the energy is smoothed (on a scale $\epsilon << 1$), which yields the expression $\mathcal{E}_\epsilon$ depending on ϕ, η and $\overline{J}$:

$$\mathcal{E}_\epsilon(t) = \int_\Omega E(|\nabla\phi(t,\mathbf{x})|\overline{J}(t,\mathbf{x}))\frac{1}{\epsilon}\zeta(\frac{\phi(t,\mathbf{x})}{\epsilon})\eta^+(t,\mathbf{x})\overline{J}^{-1}(t,\mathbf{x})d\mathbf{x}, \tag{2.24}$$

the term $\frac{1}{\epsilon}\zeta(\frac{\phi(t,x)}{\epsilon})|\nabla\phi|$ being an approximation of the Dirac mass on Γ_t.

Practically, we take $\epsilon = 2\delta$, where δ is the typical spatial step. The smoothing function ζ is classically defined by:

$$\zeta(y) = \begin{cases} \frac{1}{2}(1+\cos\pi y) & \text{if } |y|<1, \\ 0 & \text{otherwise.} \end{cases}$$

In the sequel, we use the notation $\zeta_\epsilon(\phi) = \frac{1}{\epsilon}\zeta(\frac{\phi}{\epsilon})$.

To recover the elastic force (through Eq. (2.16)), we differentiate (2.24) w.r.t. the time variable t and get,

$$\begin{aligned}\frac{d}{dt}\mathcal{E}_\epsilon(t) = &\int_\Omega \left(E(|\nabla\phi|\overline{J})\frac{1}{\epsilon^2}\zeta'(\frac{\phi}{\epsilon})\partial_t\phi\,\eta^+\overline{J}^{-1} + E(|\nabla\phi|\overline{J})\zeta_\epsilon(\phi)\partial_t\eta^+\overline{J}^{-1}\right) d\mathbf{x} \\ &+ \int_\Omega \left(E'(|\nabla\phi|\overline{J})\partial_t(|\nabla\phi|\overline{J})\zeta_\epsilon(\phi)\eta^+\overline{J}^{-1} - E(|\nabla\phi|\overline{J})\zeta_\epsilon(\phi)\eta^+\frac{\partial_t\overline{J}}{\overline{J}^2}\right) d\mathbf{x},\end{aligned}$$

where we have

$$\partial_t(|\nabla\phi|\overline{J}) = \left(\frac{\nabla\phi}{|\nabla\phi|}\cdot\nabla(\partial_t\phi)\right)\overline{J} + |\nabla\phi|\partial_t\overline{J}.$$

Furthermore, we know that ϕ is the solution to the advection equation $\partial_t\phi + \mathbf{v}\cdot\nabla\phi = 0$ and that $\overline{J}$ satisfies $\partial_t\overline{J} + \mathbf{v}\cdot\nabla\overline{J} = (\nabla\cdot\mathbf{v})\overline{J}$.

We shall also compute the term $\partial_t\eta^+$, where we remind that η is a solution of Eq. (2.14). To perform an identification with (2.16), one has to neglect the right-hand side of (2.14). This means that we assume that the influence of the rate of degradation on the elastic force is small. We multiply this equation by $\mathbf{1}_{\{\eta>0\}}$ (the characteristic function of the set $\{\eta>0\}$) to get $\partial_t\eta^+ = -\mathbf{v}\cdot\nabla\eta^+$.

We replace $\partial_t\phi$, $\partial_t\eta^+$ and $\partial_t\overline{J}$ by their expressions in the former equations and we obtain:

$$\begin{aligned}\frac{d}{dt}\mathcal{E}_\epsilon(t) = &\int_\Omega E(|\nabla\phi|\overline{J})\frac{1}{\epsilon^2}\zeta'(\frac{\phi}{\epsilon})(-\mathbf{v}\cdot\nabla\phi)\eta^+\overline{J}^{-1} + E(|\nabla\phi|\overline{J})\zeta_\epsilon(\phi)(-\mathbf{v}\cdot\nabla\eta^+)\overline{J}^{-1}\,d\mathbf{x} \\ &+ \int_\Omega E'(|\nabla\phi|\overline{J})\left(\frac{\nabla\phi}{|\nabla\phi|}\cdot\nabla(-\mathbf{v}\cdot\nabla\phi)\right)\zeta_\epsilon(\phi)\eta^+\,d\mathbf{x} \qquad (2.25) \\ &+ \int_\Omega E'(|\nabla\phi|\overline{J})|\nabla\phi|\zeta_\epsilon(\phi)\eta^+\left(\nabla\cdot\mathbf{v} - \frac{\nabla\overline{J}}{\overline{J}}\cdot\mathbf{v}\right)d\mathbf{x} \qquad (2.26) \\ &+ \int_\Omega E(|\nabla\phi|\overline{J})\zeta_\epsilon(\phi)\eta^+\left(\frac{\nabla\overline{J}}{\overline{J}^2}\cdot\mathbf{v} - \overline{J}^{-1}\nabla\cdot\mathbf{v}\right)d\mathbf{x}. \qquad (2.27)\end{aligned}$$

In [17], this expression can be further simplified since $\nabla\cdot\mathbf{v} = 0$. In our case, this equation is no longer satisfied by $\mathbf{v}$ as shown in Eq. (2.6).

To simplify the equations we will note $\mathbf{n}_\phi = \frac{\nabla\phi}{|\nabla\phi|}$ and $\mathbf{n}_J = \frac{\nabla\overline{J}}{\overline{J}}$.

Here we assume that the membrane does not cross the boundary of computational domain. From the numerical point of view, if the membrane crosses the boundary we assume that the membrane is fixed at this point.

After integrating by parts, line (2.25) yields:

$$\int_\Omega E'(|\nabla\phi|\overline{J})\left(\mathbf{n}_\phi\cdot\nabla(-\mathbf{v}\cdot\nabla\phi)\right)\zeta_\epsilon(\phi)\eta^+\,d\mathbf{x} = \int_\Omega \nabla\cdot\left(E'(|\nabla\phi|\overline{J})\zeta_\epsilon(\phi)\eta^+\mathbf{n}_\phi\right)\nabla\phi\cdot\mathbf{v}d\mathbf{x}.$$

We compute

$$\nabla \cdot \left(E'(|\nabla\phi|\overline{J})\zeta_\epsilon(\phi)\eta^+\mathbf{n}_\phi\right) = (\nabla E'(|\nabla\phi|\overline{J})\cdot\mathbf{n}_\phi)\zeta_\epsilon(\phi)\eta^+ + E'(|\nabla\phi|\overline{J})\frac{1}{\epsilon^2}\zeta'(\frac{\phi}{\epsilon})\eta^+\nabla\phi\cdot\mathbf{n}_\phi + E'(|\nabla\phi|\overline{J})\zeta_\epsilon(\phi)\nabla\eta^+\cdot\mathbf{n}_\phi + E'(|\nabla\phi|\overline{J})\zeta_\epsilon(\phi)\eta^+\kappa(\phi),$$

where $\kappa(\phi) = \nabla\cdot\mathbf{n}_\phi$ denotes the curvature.

We will see in section 3.4 how to extend the variable η as a constant along the normals to the interface. Indeed, from a biological point of view, η is only defined on the interface and the spatial derivative in the normal direction to the interface has no meaning. Hence, we can safely assume that $\nabla\eta^+\cdot\mathbf{n}_\phi = 0$ in the former expression.

The remaining terms in $\nabla\cdot\mathbf{v}$ of (2.26) and (2.27) can be written:

$$\int_\Omega \left(E'(|\nabla\phi|\overline{J})|\nabla\phi| - \overline{J}^{-1}E(|\nabla\phi|\overline{J})\right)\zeta_\epsilon(\phi)\eta^+\nabla\cdot\mathbf{v}\,d\mathbf{x} = \int_\Omega \nabla\left((-E'(|\nabla\phi|\overline{J})|\nabla\phi|\overline{J} + E(|\nabla\phi|\overline{J}))\zeta_\epsilon(\phi)\overline{J}^{-1}\eta^+\right)\cdot\mathbf{v}d\mathbf{x}.$$

We define $\tilde{E}(x) = E'(x)x - E(x)$. We can develop

$$\begin{aligned}\nabla\left(-\tilde{E}(|\nabla\phi|\overline{J})\zeta_\epsilon(\phi)\overline{J}^{-1}\eta^+\right) =& -\frac{1}{\epsilon^2}\zeta'(\frac{\phi}{\epsilon})\tilde{E}(|\nabla\phi|\overline{J})\overline{J}^{-1}\eta^+\nabla\phi \\ &+ \zeta_\epsilon(\phi)\eta^+\tilde{E}(|\nabla\phi|\overline{J})\frac{\nabla\overline{J}}{\overline{J}^2} \\ &- \zeta_\epsilon(\phi)\tilde{E}(|\nabla\phi|\overline{J})\overline{J}^{-1}\nabla\eta^+ \\ &- \zeta_\epsilon(\phi)\overline{J}^{-1}\eta^+\nabla\tilde{E}(|\nabla\phi|\overline{J}),\end{aligned}$$

where $\nabla(|\nabla\phi|) = \frac{(\nabla\phi\cdot\nabla)\nabla\phi}{|\nabla\phi|} = (\mathbf{n}_\phi\cdot\nabla)\nabla\phi$.

Collecting the above equations, we get:

$$\begin{aligned}\frac{d}{dt}\mathcal{E}_\epsilon(t) =& \int_\Omega \eta^+\zeta_\epsilon(\phi)\left(\nabla E'(|\nabla\phi|\overline{J})\cdot\mathbf{n}_\phi + E'(|\nabla\phi|\overline{J})\kappa(\phi)\right)\nabla\phi\cdot\mathbf{v} \\ &- \int_\Omega \left(E'(|\nabla\phi|\overline{J})|\nabla\phi|\zeta_\epsilon(\psi)\right)\nabla\eta^+\cdot\mathbf{v} \\ &- \int_\Omega \zeta_\epsilon(\phi)\overline{J}^{-1}\eta^+\nabla\tilde{E}(|\nabla\phi|\overline{J})\cdot\mathbf{v}.\end{aligned}$$

The identification is straightforward, and we obtain an expression of the elastic force $\mathbf{F}$:

$$\begin{aligned}\mathbf{F} =& -\eta^+\zeta_\epsilon(\phi)\left(\nabla E'(|\nabla\phi|\overline{J})\cdot\mathbf{n}_\phi + E'(|\nabla\phi|\overline{J})\kappa(\phi)\right)\nabla\phi \\ &+ \left(E'(|\nabla\phi|\overline{J})|\nabla\phi|\zeta_\epsilon(\psi)\right)\nabla\eta^+ \\ &+ \zeta_\epsilon(\phi)\overline{J}^{-1}\eta^+\nabla\tilde{E}(|\nabla\phi|\overline{J}).\end{aligned} \tag{2.28}$$

The former expression can be further developed. In particular, one has

$$|\nabla\phi|\kappa_\phi = \Delta\phi - \mathbf{n}_\phi\cdot\nabla(|\nabla\phi|). \tag{2.29}$$

However, Eq. (2.28) can be used for the numerical simulations and has fewer terms than a complete development.

2.6. Summary of the equations to be solved. We compute the tumoral densities in the proliferating (P_1 and P_2) and quiescent (Q) phases with:

$$\left\{\begin{array}{l} \partial_t P_1 + \partial_a P_1 + \nabla\cdot(\mathbf{v}\,P_1) = 0, \\ \partial_t P_2 + \partial_a P_2 + \nabla\cdot(\mathbf{v}\,P_2) = 0, \\ \partial_t Q + \nabla\cdot(\mathbf{v}\,Q) = (1-f)P_1(a=a_{\max,P_1}) - \left[\frac{d}{dt}f\right]^+ Q(t^-), \\ P_1(a=0) = 2P_2(a=a_{\max,P_2}), \\ P_2(a=0) = f\,P_1(a=a_{\max,P_1}) + \left[\frac{d}{dt}f\right]^+ Q(t^-). \end{array}\right.$$

The oxygen concentration C evolves through:

$$\left\{\begin{array}{l} -\nabla\cdot(K\nabla C) = -\alpha\left(\sum_{i=1,2}\int_0^{a_{\max,P_i}} P_i(a)da\right)C, \text{ on } \Omega\setminus \mathrm{O}, \\ C = C_0 \text{ on } \partial\Omega, \\ C = C_{\max} \text{ on } \mathrm{O}. \end{array}\right.$$

The velocity of the motion created by the cellular division is computed (along with the pressure P) with the following equations:

$$\left\{\begin{array}{l} -\nabla\cdot(\nu D(\mathbf{v})) + \nabla\left(P + \frac{2}{d}\nu\mathrm{tr}(D(\mathbf{v}))\right) = \mathbf{F}, \\ \nabla\cdot\mathbf{v} = P_2(a_{\max,P_2}), \\ \mathbf{v}\cdot\mathbf{n} = -\frac{\partial\psi}{\partial\mathbf{n}}, \partial_n\mathbf{v}\cdot\tau = 0 \text{ on } \partial\Omega, \\ \mathbf{F} = (2.28), \end{array}\right.$$

where the function ψ satisfies:

$$\left\{\begin{array}{l} \Delta\psi = -P_2(a_{\max,P_2}), \\ \psi = 0, \text{ on } \partial\Omega. \end{array}\right.$$

The localization (ϕ) and state of degradation (η) of the membrane obey:

$$\left\{\begin{array}{l} \partial_t\phi + \mathbf{v}\cdot\nabla\phi = 0, \\ \partial_t\eta + \mathbf{v}\cdot\nabla\eta = -\beta(\mathcal{M}), \\ \partial_t\mathcal{M} - \nabla\cdot(K_{\mathcal{M}}\nabla\mathcal{M}) = \eta^+\cdot\sum_{i=1,2}\int_0^{a_{\max,P_i}} P_i(a)da - \alpha_{\mathcal{M}}\mathcal{M} \end{array}\right.$$

3. Numerical schemes. We have used a finite-volume scheme to discretize our equations. In this classical scheme [40], all the variables but the velocity are evaluated at the center of the numerical cells (squares for a 2D scheme, cubes for a 3D scheme).

Let us first introduce the notations. The quantities to be computed depend on three or four variables: the time t and the space variables x, y and z (in the three-dimensional case).

For a function u defined on the grid, we write $u^n_{i,j,k}$ for the average value of u on the cell centered at the grid point (t_n, x_i, y_j, z_k) where $t_n = n\,\delta t$, $x_i = i\,\delta x$, $y_j = j\,\delta y$, $z_k = k\,\delta z$, δt being the time step, δx, δy, δz the spatial steps.

The scheme that we have used is shown in Figure 3.1. For convenience, we have only represented the bidimensional scheme but the extension to three dimensions is straightforward.

3.1. Diffusion equation. The evolution of the oxygen distribution obeys the elliptic boundary-value problem (2.7). A penalty method is used to fix the oxygen concentration on the part O of the domain. This means that one solves

$$-\nabla\cdot(K\nabla C) + \frac{1}{\varepsilon}(C - C_{\max})\mathbf{1}_O = -\alpha\left(\sum_{i=1,2}\int_0^{a_{\max,P_i}} P_i(a)da\right)C, \tag{3.1}$$

FIG. 3.1. *A cell in the MAC scheme used in the bidimensional case.*

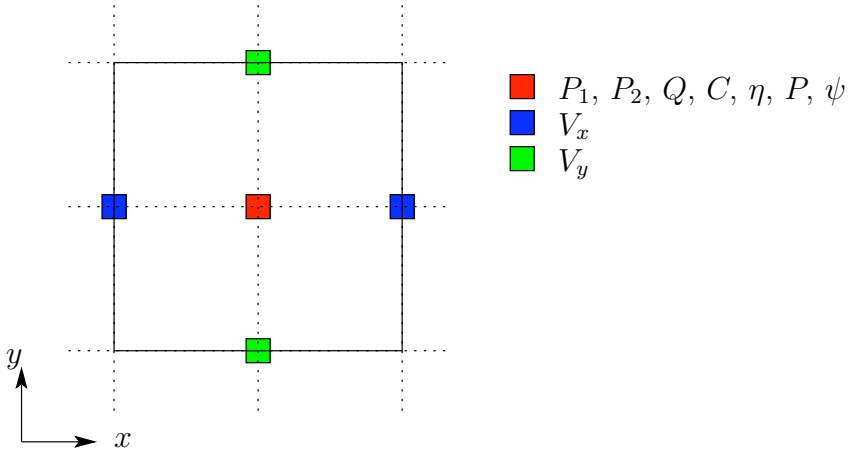

for ε small enough (in practice $\varepsilon = 10^{-10}$).

We integrate Eq. (3.1) over one cell and apply Stokes theorem. This yields a linear system (involving a five-diagonal matrix), that we have to solve at each time step. For this purpose, we use an iterative method [6, 7].

To ensure continuity of the flux, the diffusion coefficient at the boundaries of the cell is computed using the harmonic mean as follows.

For instance, in the bidimensional case, to obtain the equation on $C^{n+1}_{i+\frac{1}{2},j+\frac{1}{2}}$ (see Figure 3.1), we need the values $K^{n+1}_{i,j+\frac{1}{2}}$, $K^{n+1}_{i+1,j+\frac{1}{2}}$, $K^{n+1}_{i+\frac{1}{2},j}$ and $K^{n+1}_{i+\frac{1}{2},j+1}$.

According to Appendix A, the diffusion coefficient can be obtained in the center of the cells by:

$$K^{n+1}_{i+\frac{1}{2},j+\frac{1}{2}} \sim D_{\text{ext}}\left(\sum_a ([P_1+P_2]^n_{i+\frac{1}{2},j+\frac{1}{2}}) + Q^n_{i+\frac{1}{2},j+\frac{1}{2}}\right) - [\eta^+]^n_{i+\frac{1}{2},j+\frac{1}{2}},$$

the function D_{ext} being described in appendix A.

Then, we approximate $K^{n+1}_{i,j+\frac{1}{2}}$ by $\frac{2K^{n+1}_{i+\frac{1}{2},j+\frac{1}{2}}K^{n+1}_{i-\frac{1}{2},j+\frac{1}{2}}}{K^{n+1}_{i+\frac{1}{2},j+\frac{1}{2}}+K^{n+1}_{i-\frac{1}{2},j+\frac{1}{2}}}$ and use similar approximations for the remaining values.

3.2. Advection equations and densities evolution. To compute the elastic force, we have to compute second-order derivatives of the level set function ϕ as shown in Eq. (2.28) for instance. Hence, to have a consistent approximation of these derivatives, we need at least a second order scheme for discretizing the advection equation on the level set function.

To discretize the various advection equations (on cell densities, level set function,...), we use a fifth-order WENO discretization in space and a third-order Runge-Kutta scheme in time [25].

In the following, we briefly recall the principle of WENO schemes. The spatial derivatives have to be computed at the cells center (as the variable we wish to transport). To avoid large numerical diffusion, we need a high-order scheme to approximate the spatial derivative. To prevent instabilities, we also have to avoid areas where the

advected quantity is discontinuous. In the fifth-order WENO scheme, the numerical flux at the cell boundaries is computed as a convex combination of three 3-points stencils where each stencil is weighted according to the regularity of the function on this stencil.

The time step δt is computed at every iteration to ensure that the CFL conditions holds through:

$$\delta t = c_{\mathrm{CFL}} \min\left(\frac{\delta x}{|v_x|_\infty}, \frac{\delta y}{|v_y|_\infty}, \frac{\delta z}{|v_z|_\infty}\right), \tag{3.2}$$

where we take $c_{\mathrm{CFL}} = 0.45$ in the following.

Thanks to this accurate scheme for the advection equation, we can derive a numerical scheme for the equations leading the evolution of the cellular densities.

Let us denote by χ, the density in a particular phase χ (namely P_1 or P_2). The equation on χ is written as:

$$\partial_t \chi + \partial_a \chi + \mathbf{v} \cdot \nabla \chi + (\nabla \cdot \mathbf{v})\chi = 0.$$

Using a splitting method, we solve this equation with three steps.

In the first step , we solve $\partial_t \chi + \partial_a \chi = 0$ with an first-order upwind scheme. We use an optimal time step ($\delta t = \delta a$) since the velocity in age a is constant.

Next, for the equation $\partial_t \chi + \mathbf{v} \cdot \nabla \chi = 0$, we use the numerical scheme for the advection equations, we have just described.

Finally, we can solve $\partial_t \chi + (\nabla \cdot \mathbf{v})\chi = 0$ explicitly. Let us recall that $\nabla \cdot \mathbf{v} = P_2(a_{\max,P_2})$. We have $\chi^{n+1} = \exp(-P_2^n(a_{\max,P_2})\delta t)\chi^n$.

In equation (2.14) describing the evolution of the state of the membrane, the right-hand is evaluated at the previous time step that is to say that at time $t_{n+\frac{1}{2}}$, we take $[\beta(\eta^+ \cdot \sum_a (P_1 + P_2))]^{n+\frac{1}{2}} \sim \beta([\eta^+]^n \cdot \sum_a [P_1 + P_2]^n))$.

3.3. Stokes equation. To compute the velocity and pressure of the fluid, we have to solve the Stokes equations. The main difficulty is to ensure that the divergence of the velocity satisfies Eq. (2.6). Many methods have been developed for this problem. For instance, one can see [15, 50]. In order to ensure that we have a correct value for this divergence, we use the augmented Lagrangian method, see Fortin and Glowinski [26].

With this method, velocity and pressure are no longer coupled. Boundary conditions are not needed for the pressure term. The principle is to add a pressure term to Eq. (2.8),

$$\begin{cases} -\nabla \cdot (\nu D(\mathbf{v})) + \nabla P = \mathbf{F} \\ \epsilon_0 \partial_r P + \nabla \cdot \mathbf{v} = \sigma, \end{cases} \tag{3.3}$$

where $\sigma = P_2(a_{\max,P_2})$ and r denotes the pseudo-time step of the augmented Lagrangian method.

In Eq. (3.3), we have replaced the pressure P by $P + \frac{2}{d}\nu \mathrm{tr}(D(\mathbf{v}))$. Indeed, we have

$$\mathrm{tr}(D(\mathbf{v})) = \nabla \cdot \mathbf{v} = P_2(a_{\max}). \tag{3.4}$$

The stationary solution to (3.3), is the solution to the Stokes equations (2.8). Between two time steps, we will perform L Lagrangian iterations to approximate the stationary solution of Eq. (3.3).

Eq. (3.3) is discretized in time, (Augmented Lagrangian steps are denoted by fractional time steps):

$$\begin{cases} -\nabla \cdot (\nu D(\mathbf{v}^{n+\frac{\ell}{L}})) + \nabla P^{n+\frac{\ell}{L}} = \mathbf{F}^n, \quad 1 \leq \ell \leq L, \\ P^{n+\frac{\ell}{L}} - P^{n+\frac{\ell-1}{L}} = -r\nabla \cdot v^{n+\frac{\ell}{L}} + r\sigma^n, \end{cases} \tag{3.5}$$

where $r = \frac{dr}{\epsilon_0}$. In our computations, we took $r = 2$. We replace $P^{n+\frac{\ell}{L}}$ in the first equation by its expression obtained from the second one. Thus we get a new system, where velocity and pressure are no longer coupled:

$$\begin{cases} -\nabla \cdot (\nu D(\mathbf{v}^{n+\frac{\ell}{L}})) - r\nabla(\nabla \cdot \mathbf{v}^{n+\frac{\ell}{L}}) = -\nabla P^{n+\frac{\ell-1}{L}} + \mathbf{F}^n - r\nabla\sigma^n, \quad 1 \leq \ell \leq L, \\ P^{n+\frac{\ell}{L}} = P^{n+\frac{\ell-1}{L}} - r\nabla \cdot v^{n+\frac{\ell}{L}} + r\sigma^n. \end{cases} \tag{3.6}$$

Each equation of system (3.6) is written on a different cell. The second equation giving the pressure term $P^{n+\frac{\ell}{L}}$ is written on the cell centered on P. For the velocity components, we use staggered grids shifted by half a spatial step in the direction of the velocity component we wish to compute.

Thus, a linear system on the velocity is obtained. This system is solved at every iteration [6, 7]. Once the velocity is computed, the pressure is obtained from the last equation of (3.6).

It remains to estimate the elastic force $\mathbf{F}^n$ appearing as a source term in Eq. (3.6). We know that this force is vanishing outside the interface. At a given point $\mathbf{x}$ of the domain, we have to compute $\mathbf{F}^n$ only if $|\phi(t_n, \mathbf{x})| < \epsilon$, otherwise $\mathbf{F}^n(\mathbf{x}) = 0$.

We evaluate Eq. (2.28) at time t_n. We have to compute $[\nabla\phi]^n$, $[\nabla\eta^+]^n$, $[\nabla\overline{J}]^n$, κ_ϕ^n and $[\nabla(|\nabla\phi|)]^n$. The first-order terms $[\nabla\phi]^n$, $[\nabla\overline{J}]^n$ and $[\nabla\eta^+]^n$ are obtained through a WENO scheme as in the discretization of the advection equations (2.13) and (2.14).

The curvature $\kappa = \nabla \cdot \frac{\nabla\phi}{|\nabla\phi|}$ is computed from $[\nabla\phi]^n$ by a centered discretization.

3.3.1. Boundary conditions. In order to obtain the values of the velocity $\mathbf{v}$ at the boundary of the domain, we have to compute ψ solution of Eq. (2.10).

First, we compute ψ^{n+1} using the scheme described in section 3.1.

As the computational domain is rectangular, we have $v_x|_{0,j}^{n+1} = -[\partial_x\psi]_{0,j}^{n+1}$, $v_x|_{N_x,j}^{n+1} = -[\partial_x\psi]_{N_x,j}^{n+1}$, $v_y|_{i,0}^{n+1} = -[\partial_y\psi]_{i,0}^{n+1}$ and $v_y|_{i,N_y}^{n+1} = -[\partial_y\psi]_{i,N_y}^{n+1}$.

The spatial derivatives $\partial_x\psi$ and $\partial_y\psi$ are easily computed at the boundary of the domain using a second order approximation and the fact that ψ vanishes at the boundary.

3.4. Redistanciation and renormalization equations. The level set function ψ evolves through an advection equation (2.13). Initially, the function ϕ is the signed distance to the interface. Of course for $t > 0$, ϕ is not the distance to the interface anymore. However at each time step, we need to compute the elastic force, and to compute accurately the curvature and the normal to the level sets. This is much easier to ensure with a function that is the distance to the interface.

For this purpose, we introduce a function ϕ_d denoting the signed distance to the interface $\phi = 0$. To compute ϕ_d from ϕ we perform a redistanciation step [39] consisting in resolving an Hamilton-Jacobi equation on the level set ϕ_d:

$$\partial_\tau\phi_d + \mathrm{sgn}(\phi_0)\,(|\nabla\phi_d| - 1) = 0, \tag{3.7}$$

where ϕ_0 denotes the function ϕ at the beginning of the reinitialization step and sgn the (smoothed) sign function defined by:

$$\mathrm{sgn}(\phi_0)_{ij} = \frac{(\phi_0)_{ij}}{\sqrt{(\phi_0)_{ij}^2 + \delta x^2}}. \tag{3.8}$$

The original level set function ϕ can not be reinitialized to a signed distance as it contains information about the stretching of the membrane.

Let us note that as the sign function is vanishing for the zero level set, this equation does not modify this level set. This is true at the continuous level not at a discrete level. However as this redistanciation process is performed at each time step starting from ϕ providing the correct zero level set, in our case the error remains small and does not accumulate over time. The stationary solution to Eq. (3.7) is the signed distance to Γ_t. The principle of the redistanciation process is to replace ϕ_d by the stationary solution of Eq. (3.7). This approach was chosen for its simplicity, a more accurate method can be found in [18].

The discretization scheme is based on [33]. The term $\nabla\phi_d$ is computed using a fifth-order WENO scheme. We then use a Godunov flux, whose expression is simple in the case of (3.7). The time-integration is performed using a TVD third-order Runge-Kutta scheme [30].

The pseudo time step $\delta\tau$ depends on the spatial step, we choose to take $\delta\tau = \frac{\min(\delta x,\delta y,\delta z)}{10}$ which satisfies the CFL condition for Eq. (3.7). The reinitialization process starts from the zero level set and progresses toward the normals. Thus, only a few steps of (3.7) are needed to ensure that the function ϕ is identical to the distance function in the vicinity of the interface. Practically, a rule of thumb is that it requires a number of time steps of the order of the number of grid-points in the support of the smoothing function ζ.

Once the distance is computed, we can evaluate

$$\kappa_\phi = \nabla \cdot (\frac{\nabla\phi_d}{|\nabla\phi_d|}),\ \mathbf{n}_\phi = \frac{\nabla\phi_d}{|\nabla\phi_d|}. \tag{3.9}$$

We shall also note that the state of the extra-cellular matrix η is only defined on the zero level of the function ϕ. To compute $\nabla\eta^+$, we extend the variable on a few cells around the interface. We perform this extension along the normals of Γ_t, thus η is constant along the normals. To this aim, we replace η by an approximation of the stationary solution to the following equation [51]:

$$\partial_\tau\eta + \mathrm{sgn}(\phi_d)\frac{\nabla\phi_d}{|\nabla\phi_d|}\cdot\nabla\eta = 0, \tag{3.10}$$

where sgn is defined in Eq. (3.8). As for the redistanciation equation, we use a WENO scheme to compute the spatial derivatives and a TVD Runge-Kutta scheme for the temporal discretization.

4. Numerical Experiments. To save computational time, we use a sub-cycling method. Indeed, the typical time-scales of all the phenomena are not the same. This is summarized in Table 4.1.

The various parameters used are listed in Table A.1 of Sec. A. We took the total number of cells per unit volume N_0 (see Eq. (2.5)) equals to 1.

TABLE 4.1
Time scales of the various biological phenomena.

Scale	Phenomenon	Typical value
Cell Cycle	Cellular division	1
Cellular scale	Diffusion – Degradation	$\frac{1}{10}$
Fluid Scale	Stokes – Advection	$\frac{1}{100}$

4.1. Environmental and external conditions. In the following experiments, we use the experimental setup shown in Figure 4.1. We have plotted the interface $|\phi| = 0$ (while numerically it should be $|\phi| < \epsilon$). The level set function ϕ is initialized to the signed distance to the interface. The basal membrane is initially not degraded, hence we have $\eta^0_{i+\frac{1}{2},j+\frac{1}{2},k+\frac{1}{2}} = 1$ if $|\phi^0_{i+\frac{1}{2},j+\frac{1}{2},k+\frac{1}{2}}| < \epsilon$ and η^0 is vanishing elsewhere.

FIG. 4.1. *Experimental setup. The membrane (plotted in white) divides the domain in two parts. The oxygen supply (in green) can be found in the upper part of the domain, while the initial tumor is in the lower part. The color bar describes the tumor cells density.*

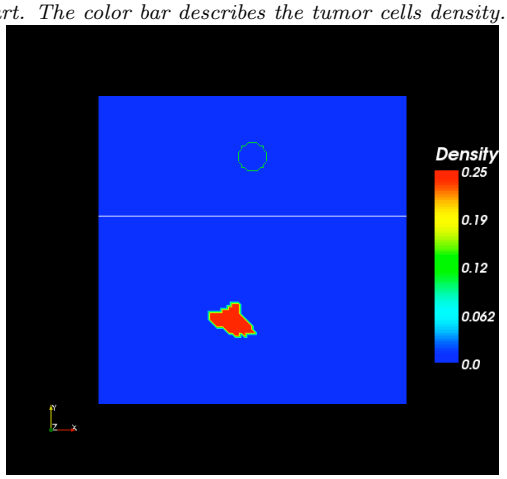

The inital tumoral distribution was taken from a scan image of a lung cancer (courtesy David Sarrut, Centre Léon Bérard, Lyon, France). Initially, all the tumor cells are uniformly distributed between proliferating phases.

4.1.1. Hypoxia. In this section, we study the effect of the lack of oxygen on the tumor growth. We neglect the overpopulation factor (*i.e.* $\tau_o > N_0$).

The experimental setup is the following. We have taken the threshold of hypoxia $\tau_o = 0.2$. For this run, we have used a 100×100 grid. The spatial step is equal to 0.08 for both dimensions. We use a CFL condition of 0.45. The experiment is run until $T = 120$. The initial tumor was obtained from a scan image. We have taken $C_{\max} = 10$ in Eq. (2.7).

In Figure 4.2, we have plotted the density of total tumoral density and the proliferative density at the end of the experiment.

We observe the growth of the tumor in the direction of the oxygen supply. Indeed, at the beginning of the experiment, the cells undergo mitosis and the tumor is growing. However, as there are more and more proliferating cells, the consumption of oxygen

FIG. 4.2. *Total and proliferative tumoral density at the end of the experiment. We have shown in green two isolines ($C = 0.2$ and $C = 10$) of the oxygen concentration C. In this experiment, cellular division is only controlled by the oxygen concentration.*

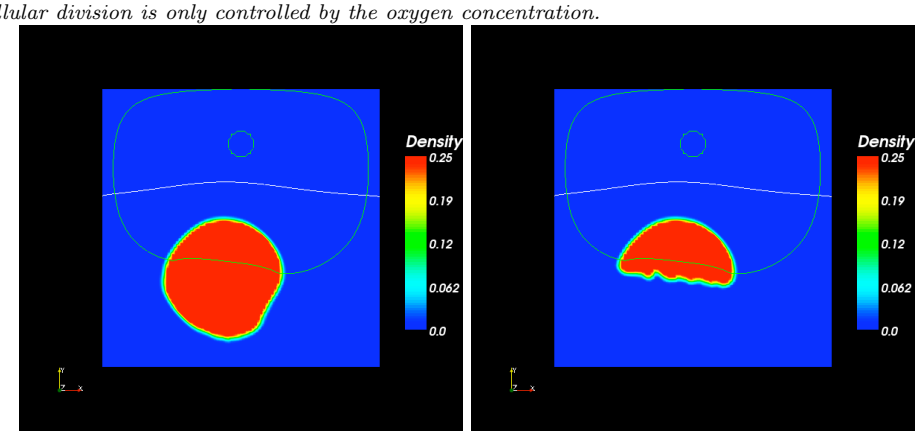

rises thus lowering the concentration. The hypoxia threshold is overpassed and many cells become quiescent.

We observe that far from the oxygen supply, the tumors cells are massively quiescent and do not participate in the tumor growth. In regions with higher oxygen concentration, the tumor is still expanding. The mitotic cells are found in the closest part of the tumor to the oxygen well.

Thus the distribution of the oxygen sources has a great influence on the shape of the tumor. Simpler models using a constant logistic growth term can not render this evolution of the shape. A realistic modeling of cellular division has to account for nutrients and their distribution. As the oxygen distribution is really smooth (one single circular source), the shape of the tumor is smoothed during the growth. This may not be the case in realistic setups or experiments as shown in [19].

4.1.2. Overpopulation. We will now study the effect of overcrowding on the tumor growth. We do not consider the hypoxia effect, so the hypoxia threshold is vanishing ($\tau_h = 0$). The overpopulation threshold is $\tau_o = 0.5N_0$.

Let us note that, as the hypoxia threshold is vanishing, the growth is isotropic.

We use the same numerical parameters as in the previous experiment.

The total density of tumor cells (in the quiescent and proliferative state) is shown in Figure 4.3.

As the tumor grows, it reaches the overpopulation threshold and the cells become quiescent. Hence, we observe that at the center of the tumor, the density appears to be lower than at its edges. As the overcrowding effect continues, it stops the growth.

At the end of the run, all the tumor cells are in the quiescent state in the center. The overpopulation threshold is not attained by outer cells, the cells are still dividing.

Let us also point out, that the shape of the tumor is completely different from the one observed in the previous section where cells undergo hypoxia. The tumor has a layered structure with a quiescent core and a proliferative rim. Contrary to other models, this structure is neither an hypothesis [27] nor enforced by a contact-inhibition term [48].

4.1.3. Elastic force. In this section, we study the effect of the surface tension on the tumor growth. For this purpose, we took two different values of T_0 in Eq.

FIG. 4.3. *Total and proliferative tumoral density at the end of the experiment. In this experiment, cellular division is only controlled by overpopulation. In particular, tumor growth does not depend on the distribution of nutrient.*

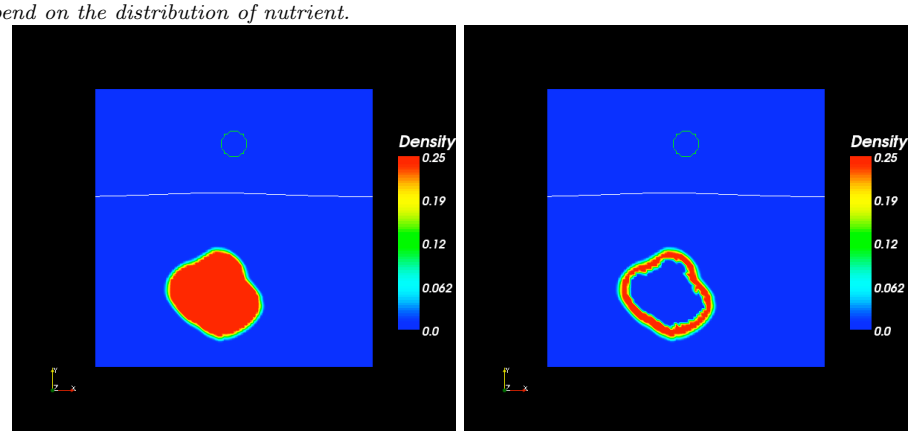

(2.15), $T_0 = 0.0$ and $T_0 = 0.1$. The experimental conditions are the following. The hypoxia and overpopulation threshold are respectively $\tau_o = 0.9N_0$, $\tau_h = 0.5$. We let the experiment run until $T = 150$. The numerical parameters are the same as in the previous runs (though in this case the initial tumor is centered on the computational domain). The position of the membrane is plotted with a plain white line.

FIG. 4.4. *Density of the cancer cells at the end of the experiment with varying elasticity of the membrane. From left to right, we present the results obtained for* $T_0 = 0.0$ *and* $T_0 = 0.1$. *The green line represents the isoline* $C = 10$ *of the oxygen concentration.*

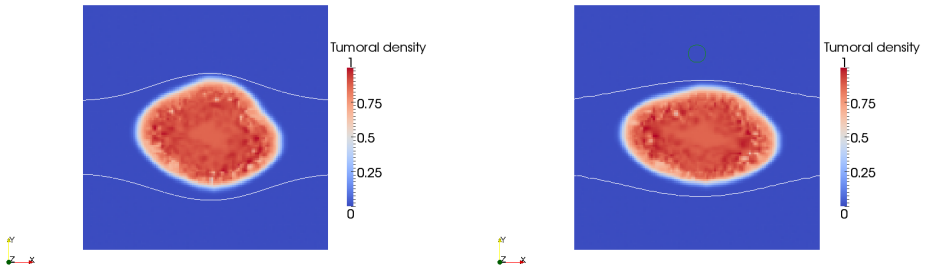

As expected, with a higher tension of the interface, the tumor shape is different. The elastic force limits the tumor expansion in the direction of the oxygen supply. The tumor extends somehow horizontally.

4.2. 3D experiments.

4.2.1. Porosity of the membrane. In this experiment, we consider a tumor separated from an oxygen supply by a membrane in three dimensions. Depending on this membrane porosity, the concentration of oxygen will vary in the domain where tumor cells stand. Thus, the rate of growth and the shape of the tumor will depend on this porosity.

The porosity of the membrane is modeled by modifying the diffusion coefficient

across the interface. In this experiment, we have considered a model with exponential growth (*i.e.* we consider only one mitotic phase, no quiescent phase, no aging and a growth rate depending on the oxygen concentration C). The initial tumor is a sphere separated from the oxygen supply by a membrane, (*i.e.* the 3D extension of the setup shown in Fig. 4.1). The results are shown on Figure 4.5.

FIG. 4.5. *Density of the tumor cells at the end of the experiment for two values of the porosity of the membrane. In the rightmost picture, we have considered a lower porosity of the membrane.*

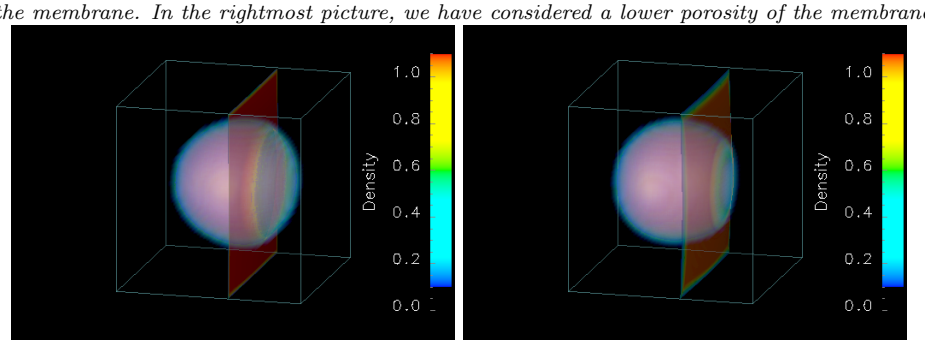

As expected, with a lower porosity, the tumor is smaller as the rate of growth depends on the oxygen distribution.

4.2.2. A complete three-dimensional case. In this section, we study the evolution of a tumor with a three-dimensional scheme with all biological features the model can integrates. This initial tumor is a spheroid. The oxygen is supplied to the tumor by a cylinder where the oxygen concentration is fixed at $C_{\max} = 15$.

We took a $74 \times 74 \times 74$ grid, which yields $\delta x = \delta y = \delta z = 0.0547945$. The two thresholds are respectively $\tau_h = 0.5$, $\tau_o = 0.8 N_0$. We let the experiment run until $T = 150$.

We have shown the density of tumoral cells and the density of quiescent cells at the end of the run on Figure 4.6.

FIG. 4.6. *Total and quiescent density of the tumoral cells at the end of the experiment of a tumor growing around a blood vessel. The oxygen supply is plotted in red.*

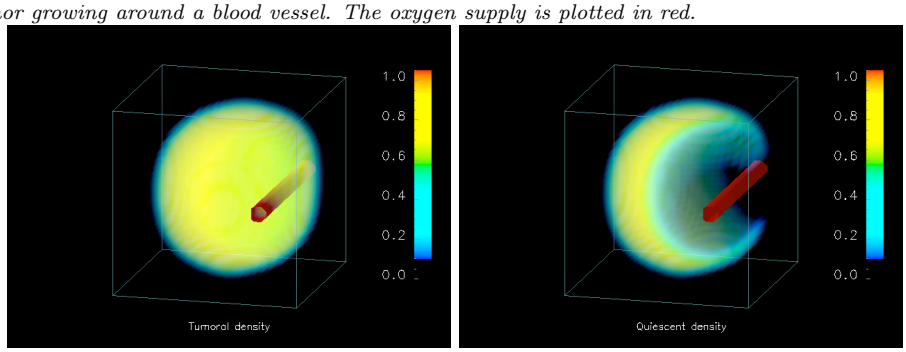

At the end of the experiment, the oxygen supply is surrounded by mitotic cells, while the outer part of the tumor is in the quiescent state: this is the formation of a tumor cord. We have not made any assumption regarding its structure contrary to [10] where an extensive mathematical study is performed.

5. Conclusion. We presented a mathematical and computational model of avascular tumor growth. With respect to existing work, our model describes with more precision both cell cycle regulation and tissue constraints which allows us to investigate qualitatively the feedback between macroscopic and microscopic levels.

This model uses a continuous approach through several PDEs based on fluid dynamics. The velocity is obtained from a Stokes equation, where the spatial expansion is translated into a constraint on the divergence of this velocity. The influence of a membrane surrounding the tumor is taken into account as a second hand term in the Stokes equation following the IMB method. Finally, to describe the tumor environment, we use a penalty method in a diffusion equation on the oxygen concentration. We are presently working on a model including tissue elasticity.

From a computational point of view, the model has been implemented with a spirit of modularity making very easy the implementation of supplement biological phenomena such as, for instance, the role of acidity on cell cycle regulation. In fact, the present work constitutes a computational platform for integrating a maximum of biological knowledge on cancer growth. The significant next step will be to implement the angiogenesis process which will allow us to propose tumor growth models for both avascular and vascular stages [11].

Acknowledgments. The authors thank Georges-Henri Cottet and Emmanuel Maître for all their comments and remarks. We also thank the referees for their useful corrections and remarks.

BR has been partially funded by the ETOILE project: "Espace de Traitement Oncologique par Ions Légers dans le cadre Européen".

OS acknowledges stimulating discussions with Pierre Fabrie (Institut de Mathématiques de Bordeaux).

REFERENCES

[1] T. Alarcón, H. M. Byrne, and P. K. Maini. A cellular automaton model for tumour growth in inhomogeneous environment. *J. Theoret. Biol.*, 225(2):257–274, 2003.

[2] B. Alberts, D. Bray, J. Lewis, M. Raff, K. Roberts, and J.D. Watson. *Molecular Biology of the Cell.* Garland Publishing, New York and London, 1994.

[3] D. Ambrosi and L. Preziosi. On the closure of mass balance models for tumor growth. *Math. Models Methods Appl. Sci.*, 12(5):737–754, 2002.

[4] A.R.A. Anderson and M.A.J. Chaplain. Continuous and discrete mathematical models of tumor-induced angiogenesis. *Bulletin of Mathematical Biology*, 60(5):857–899, 1998.

[5] A.R.A. Anderson, A.M. Weaver, P.T. Cummings, and V. Quaranta. Tumor morphology and phenotypic evolution driven by selective pressure from the microenvironment. *Cell*, 127(5):905–915, 2006.

[6] Satish Balay, William D. Gropp, Lois C. McInnes, and Barry F. Smith. Petsc home page. http://www.mcs.anl.gov/petsc, 2001.

[7] Satish Balay, William D. Gropp, Lois C. McInnes, and Barry F. Smith. Petsc users manual. Technical Report ANL-95/11 - Revision 2.1.3, Argonne National Laboratory, 2002.

[8] R.C. Bast, D.W. Kufe, R.E. Pollock, R.R. Weichselbaum, and J.F. Holland. *Cancer Medicine.* BC Decker Inc, Canada, 2000.

[9] G. Bayada and M. Chambat. Conditions aux limites à l'interface d'un milieu poreux et d'un écoulement libre de faible épaisseur. *Comptes rendus de l'Académie des sciences. Série 1, Mathématique*, 315(4):491–495, 1992.

[10] A. Bertuzzi, A. D'Onofrio, A. Fasano, and A. Gandolfi. Regression and regrowth of tumour cords following single-dose anticancer treatment. *Bulletin of mathematical biology*, 65(5):903–931, 2003.

[11] F. Billy, B. Ribba, O. Saut, H. Morre-Trouilhet, T. Colin, D. Bresch, J.P. Boissel, E. Grenier, and J.P. Flandrois. A pharmacologically based multiscale mathematical model of angio-

genesis and its use in investigating the efficacy of a new cancer treatment strategy. *Journal of Theoretical Biology*, 260(4):545–562, 2009.

[12] MV Blagosklonny and AB Pardee. The restriction point of the cell cycle. *Cell Cycle*, 1(2):103–10, 2002.

[13] D Bresch, T Colin, E Grenier, B Ribba, and O Saut. A viscoelastic model for avascular tumor growth. to appear in AIMS Proc, 2009.

[14] H. Byrne and L. Preziosi. Modelling solid tumour growth using the theory of mixtures. *Mathematical Medicine and Biology*, 20(4):341–366, 2003.

[15] Alexandre Joel Chorin. A numerical method for solving incompressible viscous flow problems [J. Comput. Phys. **2** (1967), no. 1, 12–36]. *J. Comput. Phys.*, 135(2):115–125, 1997. With an introduction by Gerry Puckett, Commemoration of the 30th anniversary {of J. Comput. Phys.}.

[16] J. Clairambault, B. Laroche, S. Mischler, and B. Perthame. A mathematical model of the cell cycle and its control. Rapport de recherche 4892, INRIA, 2003.

[17] Georges-Henri Cottet and Emmanuel Maitre. A level-set formulation of immersed boundary methods for fluid-structure interaction problems. *C. R. Math. Acad. Sci. Paris*, 338(7):581–586, 2004.

[18] G.H. Cottet, E. Maitre, and P. Degond. A level set method for fluid-structure interactions with immersed surfaces. *Mathematical Models and Methods in Applied Sciences*, 16(3):415–438, 2006.

[19] V. Cristini, H.B. Frieboes, R. Gatenby, S. Caserta, M. Ferrari, and J. Sinek. Morphologic instability and cancer invasion. *Clinical Cancer Research*, 11(19):6772, 2005.

[20] V. Cristini, X. Li, J.S. Lowengrub, and S.M. Wise. Nonlinear simulations of solid tumor growth using a mixture model: invasion and branching. *Journal of Mathematical Biology*, 58(4):723–763, 2009.

[21] V. Cristini, J. Lowengrub, and Q. Nie. Nonlinear simulation of tumor growth. *Journal of Mathematical Biology*, 46(3):191–224, 2003.

[22] E. De Angelis and L. Preziosi. Advection-diffusion models for solid tumour evolution in vivo and related free boundary problem. *Mathematical Models and Methods in Applied Sciences*, 10(3):379–408, 2000.

[23] J. Dyson, E. Sánchez, R. Villella-Bressan, and G. Webb. An age and spatially structured model of tumor invasion with haptotaxis. *DISCRETE AND CONTINUOUS DYNAMICAL SYSTEMS SERIES B*, 8(1):45, 2007.

[24] J. Dyson, R. Villella-Bressan, and G. Webb. A spatial model of tumor growth with cell age, cell size, and mutation of cell phenotypes. *Mathematical Modelling of Natural Phenomena*, 2(3):69–100, 2007.

[25] Ronald P. Fedkiw, Barry Merriman, and Stanley Osher. Simplified discretization of systems of hyperbolic conservation laws containing advection equations. *J. Comput. Phys.*, 157(1):302–326, 2000.

[26] Michel Fortin and Roland Glowinski. *Méthodes de lagrangien augmenté*, volume 9 of *Méthodes Mathématiques de l'Informatique [Mathematical Methods of Information Science]*. Gauthier-Villars, Paris, 1982. Applications à la résolution numérique de problèmes aux limites. [Applications to the numerical solution of boundary value problems].

[27] Avner Friedman. A hierarchy of cancer models and their mathematical challenges. *Discrete Contin. Dyn. Syst. Ser. B*, 4(1):147–159, 2004. Mathematical models in cancer (Nashville, TN, 2002).

[28] R.A. Gatenby. A reaction-diffusion model of cancer invasion. *Cancer Research*, 56(24):5745–5753, 1996.

[29] R.A. Gatenby and R.J. Gillies. Why do cancers have high aerobic glycolysis? *Nature Reviews Cancer*, 4(11):891–899, 2004.

[30] Sigal Gottlieb and Chi-Wang Shu. Total variation diminishing Runge-Kutta schemes. *Math. Comp.*, 67(221):73–85, 1998.

[31] D. Hanahan and R.A. Weinberg. The Hallmarks of Cancer. *Cell*, 100(1):57–70, 2000.

[32] C. Hogea, C. Davatzikos, and G. Biros. An image-driven parameter estimation problem for a reaction–diffusion glioma growth model with mass effects. *Journal of Mathematical Biology*, 2007. In press.

[33] Guang-Shan Jiang and Danping Peng. Weighted ENO schemes for Hamilton-Jacobi equations. *SIAM J. Sci. Comput.*, 21(6):2126–2143 (electronic), 2000.

[34] JR King and SJ Franks. Mathematical modelling of nutrient-limited tissue growth, in "Free Boundary Problems". *Internat. Ser. Numer. Math., Birkh "auser*, 5:273–282, 2007.

[35] P. Macklin and J. Lowengrub. Evolving interfaces via gradients of geometry-dependent inte-

rior Poisson problems: application to tumor growth. *Journal of Computational Physics*, 203(1):191–220, 2005.
[36] P. Macklin, S. McDougall, A.R.A. Anderson, M.A.J. Chaplain, V. Cristini, and J. Lowengrub. Multiscale modelling and nonlinear simulation of vascular tumour growth. *Journal of Mathematical Biology*, 58(4):765–798, 2009.
[37] Y. Mansury, M. Kimura, J. Lobo, and T.S. Deisboeck. Emerging Patterns in Tumor Systems: Simulating the Dynamics of Multicellular Clusters with an Agent-based Spatial Agglomeration Model. *Journal of Theoretical Biology*, 219(3):343–370, 2002.
[38] N.V. Mantzaris, S. Webb, and H.G. Othmer. Mathematical modeling of tumor-induced angiogenesis. *Journal of Mathematical Biology*, 49(2):111–187, 2004.
[39] Stanley Osher and Ronald Fedkiw. *Level set methods and dynamic implicit surfaces*, volume 153 of *Applied Mathematical Sciences*. Springer-Verlag, New York, 2003.
[40] S.V. Patankar. *Numerical Heat Transfer and Fluid Flow*. Hemisphere Publishing Corporation, 1980.
[41] Charles S. Peskin. The immersed boundary method. *Acta Numer.*, 11:479–517, 2002.
[42] MJ Plank, BD Sleeman, and PF Jones. A mathematical model of tumour angiogenesis, regulated by vascular endothelial growth factor and the angiopoietins. *Journal of theoretical biology*, 229(4):435–454, 2004.
[43] CS Potten, M. Kellett, SA Roberts, DA Rew, and GD Wilson. Measurement of in vivo proliferation in human colorectal mucosa using bromodeoxyuridine. *Gut*, 33(1):71–78, 1992.
[44] DA Rew, GD Wilson, I. Taylor, and PC Weaver. Proliferation characteristics of human colorectal carcinomas measured in vivo. *Br J Surg*, 78(1):60–6, 1991.
[45] B. Ribba, T. Colin, and S. Schnell. A multiscale mathematical model of cancer, and its use in analyzing irradiation therapies. *Theoretical Biology and Medical Modelling*, 3(1):7, 2006.
[46] B. Ribba, O. Saut, T. Colin, D. Bresch, E. Grenier, and J.P. Boissel. A multiscale mathematical model of avascular tumor growth to investigate the therapeutic benefit of anti-invasive agents. *J. Theoret. Biol.*, 243(4):532–541, 2006.
[47] T. Roose, S.J. Chapman, and P.K. Maini. Mathematical Models of Avascular Tumor Growth. *SIAM Review*, 49(2):179–208, 2007.
[48] J.A. Sherratt and M.A.J. Chaplain. A new mathematical model for avascular tumour growth. *Journal of Mathematical Biology*, 43(4):291–312, 2001.
[49] KR Swanson, EC Alvord Jr, and JD Murray. Virtual brain tumours (gliomas) enhance the reality of medical imaging and highlight inadequacies of current therapy. *British Journal of Cancer*, 86:14–18, 2002.
[50] Roger Temam. *Navier-Stokes equations*, volume 2 of *Studies in Mathematics and its Applications*. North-Holland Publishing Co., Amsterdam, revised edition, 1979. Theory and numerical analysis, With an appendix by F. Thomasset.
[51] Jian-Jun Xu, Zhilin Li, John Lowengrub, and Zhao Hongkai. A level-set method for interfacial flows with surfactant. *J. Comput. Phys.*, 212(2):590–616, 2006.

Appendix A. Numerical parameters and functions.

Note that it is impossible to have precise values for the functions and parameters. Most of the quantities that we consider are taken in order to obtain behavior that are concordant to biological and medical values. A way to recover the information would be to use image-driven simulation in the spirit of [32].

The coefficient K leading the diffusion of oxygen in Eq. (2.7) is obtained from the tumoral density and the position and degradation of the membrane:

$$K(t,\mathbf{x}) = D_{\text{ext}}\left(\sum_a (P_1+P_2)+Q\right) - \eta^+, \tag{A.1}$$

where the function D_{ext} has the following expression

$$D_{\text{ext}}(z) = \frac{D_0+D_1}{2} - \frac{D_0-D_1}{2}\tanh(\frac{z-D_{50}}{D_2}), \tag{A.2}$$

with $D_0 = 5$, $D_1 = 2$, $D_{50} = \frac{1}{2}$ and $D_2 = \frac{1}{20}$. This means that the diffusion coefficient of oxygen is smaller in the tumor than in sane tissue and that the membrane inhibits the diffusion of oxygen.

The function β in (2.14) is defined as

$$\beta(z) = \beta_{\max} + \beta_{\max} \tanh(20(z-4)), \tag{A.3}$$

where $\beta_{\max} = 5$.

The viscosity in equation (2.8) has the following expression:

$$\nu(t,\mathbf{x}) = \frac{2 - \frac{1}{N_0}[Q(t,\mathbf{x}) + \sum_{i=1,2} \int_0^{a_{\max,P_i}} P_i(t,\mathbf{x})da]}{2},$$

this means that the presence of tumor cells decreases the viscosity. Indeed the cancer cells are more soluble than healthy cells.

On Table A.1, we list the various numerical parameters used in our computations.

TABLE A.1
Numerical parameters used in our computations.

Description	Parameter	Value
Duration of the phase P_1	$a_{\max,P_1}$	10
Duration of the phase P_2	$a_{\max,P_2}$	6
Length of the domain	L_d	8
Width of the domain	D_d	8